Korean J. Chem. Eng., 33(10), 2869-2877 (2016)
DOI: 10.1007/s11814-016-0153-z

pISSN: 0256-1115
eISSN: 1975-7220

Density functional theory study on Hg removal mechanisms of Cu-impregnated activated carbon prepared by simplified method

Yaming Fan*, Yuqun Zhuo*,†, Zhenwu Zhu*, Liangliang Li, Qun Chen*, and Yu Lou***

*Key Laboratory for Thermal Science and Power Engineering of Ministry of Education, Department of Thermal Engineering, Tsinghua University, Beijing 100084, China
**Key Laboratory of Advanced Materials, Department of Material Science and Engineering, Tsinghua University, Beijing 100084, China
(*Received 1 December 2015 • accepted 8 June 2016*)

Abstract−The preparation of activated carbon sorbent for Hg removal was simplified by combining activation and functionalization processes into one step. Jujube-based carbon material was first mixed with $CuCl_2$ solution and then activated for the preparation of Cu-impregnated activated carbon. Physical and chemical properties of prepared activated carbon were investigated by means of N_2 adsorption, SEM-EDS, XRD. A fixed-bed reactor with CEMS (Continuous emission monitoring system) was used to test the Hg adsorption ability of prepared activated carbon. DFT (Density functional theory) method of computational chemistry calculation was applied to identify the Hg adsorption mechanisms on sorbent surface.

Keywords: One-step Preparation, Activated Carbon, Cu-impregnated, Hg Removal, Density Functional Theory

INTRODUCTION

Hg and its compounds have strong biological toxicity to the human neural system, internal organs and fetuses [1]. Coal combustion has been considered as the largest anthropogenic emission source of Hg [2]. Through a series of comprehensive studies in both laboratory-scale and industrial-scale, activated carbon injection (ACI) has been adopted in the US as a stable and efficient way to remove Hg in flue gas [3]. It has been reported that 47.7% (installed capacity) of American coal-fired power plants have applied ACI technology for the removal of Hg [4].

However, the cost of activated carbon sorbent has been a key factor limiting itself from being applied on a larger and wider scale. According to a survey in six coal-fired power plants by the National Energy Technology Laboratory (NETL) of the U.S. Department of Energy (DOE), the cost of removing 90% of Hg in flue gas by ACI was as high as 0.37-0.99 cents/kWh [5]. Generally, this type of activated carbon is made in two steps. First, carbon materials are activated under high temperature (600-1,200 °C), forming activated carbon. Then the activated carbons are functionalized (impregnation, sol-gel, etc.) by combining appropriate functional agents such as metal oxides or halogens [6]. In the second step, chemical activation is a popular method which helps to increase the surface area and porosity of the products [7]. During this step, carbon material mixed with chemical agents is heated under activation atmosphere, such as CO_2 or water vapor. The residue of chemical agents is cleared by water afterwards.

Previous researches revealed that chemical agents (e.g., $FeCl_3$) could accelerate the activation of carbon as Fe and its oxides could be impregnated on the surface of activated carbon [8]. In the meantime, some experiments by other researchers also suggested that activated carbon impregnated by CuOx was a capable Hg sorbent [9]. The preparation of activated carbon for Hg removal could be simplified by combining activation and functionalization into one-process preparation. In this study, an attempt was made by adding $CuCl_2$ into carbon materials before activation. We had expected that $CuCl_2$ could enhance the activation and enable Cu and its corresponding oxides being supported on the surface so as to promote the adsorption of Hg. The morphological characteristics of the sorbents were investigated. A fixed-bed reactor system was used to test the capability of prepared activated carbon for adsorption of Hg. Commercial sorbents such as Norit-FGD and Norit-LH were chosen for comparison purposes. Considering the low concentration of Hg in gas ($\mu g/m^3$) and solid (0.1%wt), density functional theory (DFT) method of computational chemistry was applied to investigate the Hg adsorption mechanisms in detail.

EXPERIMENTAL METHODS

1. Sorbent Preparation

Jujube-based carbon material was acquired from Hebei province of China. It was made from jujube shells carbonized under inert atmosphere before being sold in market. The sorbent preparation procedure was as follows:

i) Raw carbon material was sieved, samples between 10 and 40 mesh were collected;

ii) 30 g of collected sample was mixed with 30 ml 5% or 10% $CuCl_2$ solution, stirred at room temperature for 6 hours and stood for 3 hours, then the samples were dried in an oven at 50 °C for 3 hours;

†To whom correspondence should be addressed.
E-mail: zhuoyq@tsinghua.edu.cn

iii) Samples were then put into a 36 mm diameter quartz tube and heated under 1 L/min N_2 flow with the heat-up rate of 30 °C/s. After reaching the pre-set activation temperature (i.e., 600, 700, 800 or 900 °C), the samples were held under the same temperature with 2 L/min CO_2 flow for 2 hours. Finally, the activated carbon was cooled to room temperature under N_2.

iv) The prepared activated carbon was sieved and samples between 100-400 mesh were collected and stored for further Hg capture performance test.

The prepared samples were named by their activation temperature and the Cu content in solution; for example, '600-5' represented the sample activated under 600 °C after being mixed with 5% $CuCl_2$ solution.

2. Apparatus

A fixed bed reactor system was set up and fabricated, as shown in Fig. 1. The experimental system consisted of four parts: gaseous Hg generator, reactor, measurement and tail gas treatment.

The gaseous Hg (Hg^0) was generated by 10.534 mercury generator (PS Analytical Company, UK). Saturated Hg vapor could be diluted to obtain a wide range of Hg concentration (100 ng/m^3-300 μg/m^3). The Hg concentration in gas streams was monitored by an online continuous Hg analyzer (Mercury Freedom, Thermo Fisher, USA). The Hg content in sorbents was analyzed by Lumex RA-915M (Lumex, Russia) after each experiment. To avoid unnecessary Hg losses due to surface adsorption, all the tubes, joints, and valves were made of either quartz or Teflon.

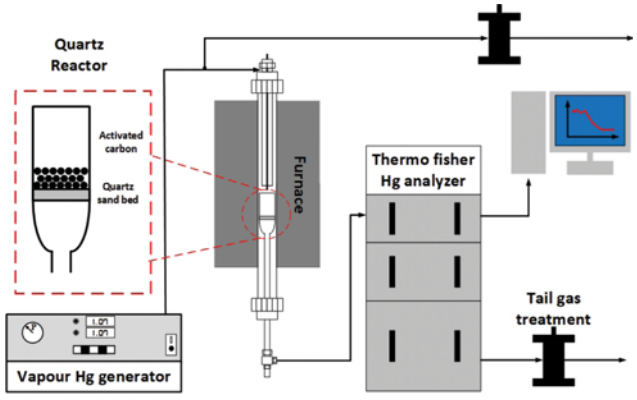

Fig. 1. Gaseous Hg adsorption experimental system.

The fixed-bed reactor was made of a 36 mm (inside diameter) quartz tube heated by a furnace. The gaseous Hg carried by N_2 passed through the fixed bed where the tested sorbents were put on. The temperature of the reactor was monitored by a thermocouple covered by quartz tube inserted in the reaction zone.

500 mg sorbent (100-400 mesh) mixed with 4,500 mg quartz sand was put into the reactor in each test. The carrier gas was 1 L/min N_2 containing 30 μg/m^3 Hg. The detailed configuration of the reactor system and operating procedures is described elsewhere [10].

3. Sorbent Characterization

The specific surface area and pore size of the sorbent were determined by an automatic N_2 adsorption analyzer (Micromeritics ASAP 2010). The crystallized species on the sorbent surface was determined by an X-ray diffractometer (XRD, Bruker D8 advance, German) with Cu Kα radiation. Transmission electron microscopy (TEM) and energy dispersive spectrometry (EDS) were applied with field emission (SEM JSM-6301-F, Japan) to investigate the surface's morphology and existing elements of the sorbent.

RESULTS AND DISCUSSION

1. Sorbent physical Characterization

The μ representing the yield of activated carbon was defined as follows:

$$\mu = \frac{m_{final}}{m_{initial}} \times 100\% \quad (1)$$

where m_{final} and $m_{initial}$ represent, respectively, the mass of prepared activated carbon and the initial mass of carbon material, includ-

Table 1. Physical Characteristics of prepared activated carbon

Sample	Surface area S_{BET} (m^2/g)	Pore volume V_{total} (cm^3/g)	Average radius of pore R (nm)	Yield μ (%)
Carbon material	3.7	0.6 E-2	/	/
600	231.4	9.3 E-2	18.7	83.9
700	292.8	14.9 E-2	19.1	80.8
800	414.3	22.3 E-2	19.0	75.1
900	627.9	60.6 E-2	19.8	41.2
600-5	302.1	12.0 E-2	19.2	83.2
600-10	307.2	13.3 E-2	17.8	83.2
700-5	276.4	10.9 E-2	19.0	78.7
700-10	290.7	12.5 E-2	18.5	79.2
800-5	357.5	14.7 E-2	19.2	73.9
800-10	381.3	15.7 E-2	19.2	71.4
900-5	433.9	17.6 E-2	19.2	42.5
900-10	486.3	19.5 E-2	19.1	40.7
Norit LH	405.0	42.0 E-2	4.2	/
Norit FGD	664.8	49.0 E-2	2.9	/

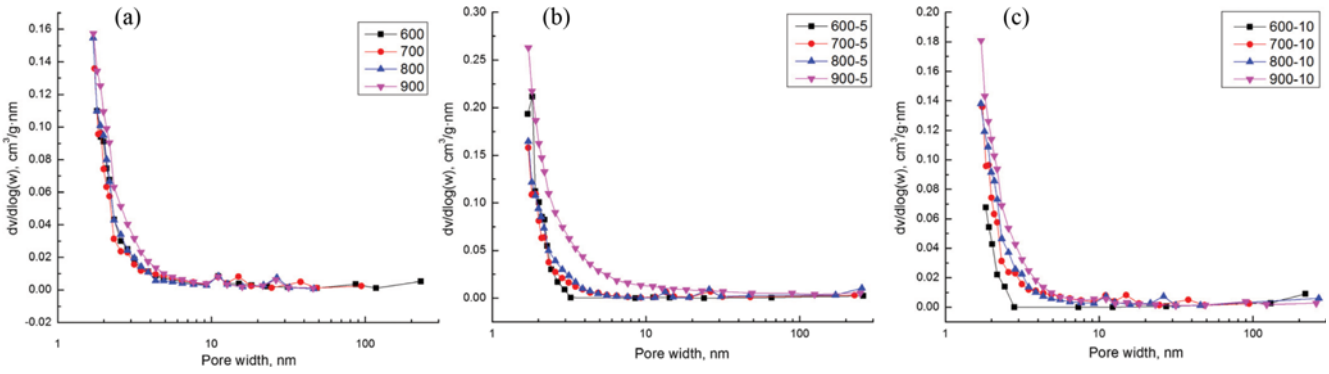

Fig. 2. Pore size distribution of prepared activated carbons.

ing the solid mass of $CuCl_2$ in solution.

Table 1 shows the physical characteristics of activated carbon under different conditions. Temperature is a key factor for carbon activation. Under the same condition, with the temperature increased from 600 °C to 900 °C, the surface area and total pore volume increased significantly while the yield decreased. This was due to the temperature acceleration of the reaction between CO_2 and C to form CO [11]. Except '600-5' and '600-10', the functionalized activated carbon's surface area and pore volume were lower (0.7-30.7%) than those of the pure activated carbon made by the same process. However, the surface area and pore volume of '600-5' and '600-10' were significantly higher than those of '600' (surface area 30.6-32.8%, pore volume 29.0%-43.0%). It suggested that the promotion of activate carbon structure already started at 600 °C. The surface area and pore volume of 'X-10' was higher than that of 'X-5' (X=600, 700, 800, 900). The pore distribution of activated carbons is shown in Fig. 2. The pore of activated carbons mostly concentrated on micro pore (1-3 nm). The Cu/Carbon ratio might influence activation effect to some extent. On the one hand, Cu compounds could promote the activation process. On the other hand, the Cu compounds might block the micro pore. So Cu/Carbon should be optimized during actual production process.

2. Sorbent Chemical Characterization

For commercial sorbents of Norit FGD (pure activated carbon) and Norit LH (brominated activated carbon), their chemical characteristic was studied [12,13].

For our prepared sorbent, we found that the major chemical elements and surface chemical characteristic were consistent under different prepared temperatures. 800 °C was chosen as a reference temperature, non-functionalized and functionalized activated carbons prepared under this temperature were compared to investigate the surface chemistry characteristic.

2-1. Morphology and Surface Elemental Analysis

Fig. 3 demonstrates the SEM and EDS images of sample surface. The pores created by CO_2 can be clearly recognized at the smooth carbon surface. Since the brightness of EDS image is related to relative atomic mass, the difference among elements can be directly identified from the images. Table 2 shows the molar ratio of elements at each measure point. For carbonized sample of '800' (non-functionalized), the major elements were C, O and Ca. Apart from C, O and Ca, Cu mainly existed on the surface of '800-5' and '800-10' while nearly no Cl was observed. Cl was chemically active; during high temperature it was reasonable to believe that Cl was volatile and could hardly exist on the solid surface. No obvious difference

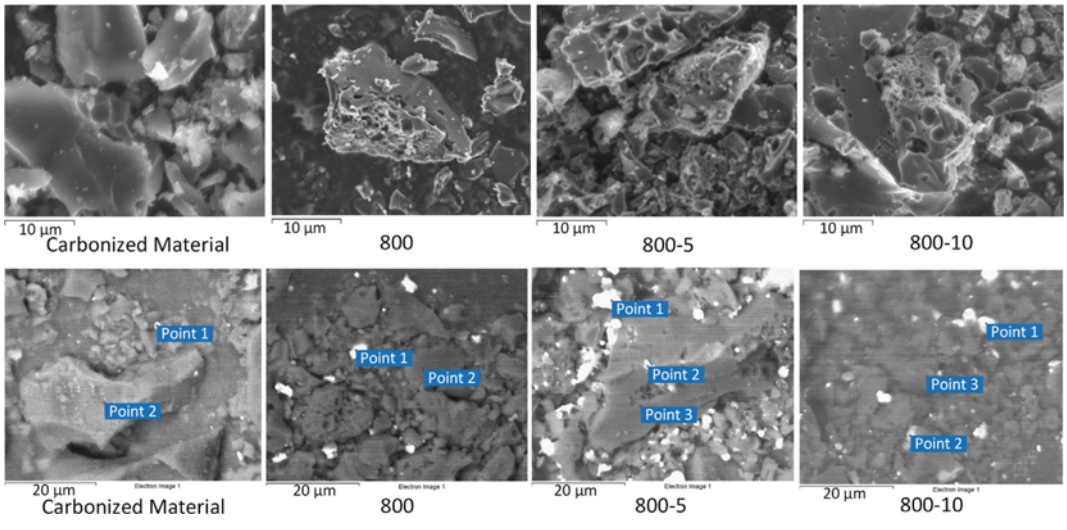

Fig. 3. SEM and EDS image of sample surface (up: SEM, down: EDS).

Table 2. Molar ratio of different elements on sample surface

Material	Measure point	Element (molar ratio, %)								
		C	O	Cu	Cl	Ca	K	Si	Mg	P
Carbonized material	1	67.0	28.3	/	/	4.1	0.1	/	0.5	/
	2	92.3	6.7	/	/	/	1.0	/	/	/
800	1	52.7	33.3	0	/	14.0	/	/	/	/
	2	93.9	6.1	0	/	/	/	/	/	/
800-5	1	67.9	4.4	27.3	/	0.3	/	/	/	/
	2	/	74.1	1	2	14.6	0.6	1.2	1.2	5.5
	3	95.4	3.8	0.2	0.2	0.3	/	/	/	/
800-10	1	68.1	4.6	27.3	/	/	/	/	/	/
	2	58.1	29.1	/	0.3	12.5	/	/	/	/
	3	96.7	3.2	/	/	/	/	/	/	/

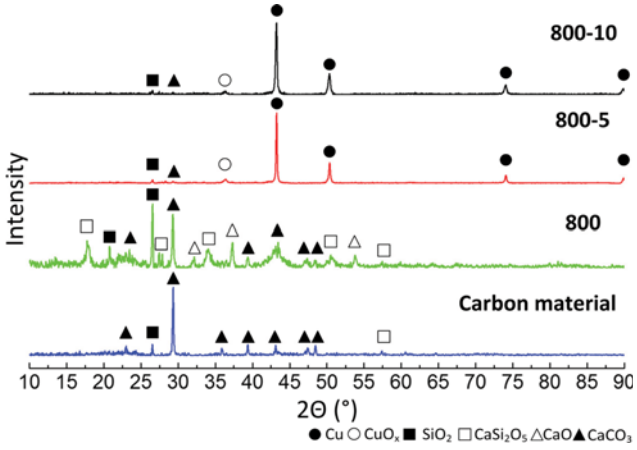

Fig. 4. XRD analysis for sorbents: carbon material (blue), 800 (green), 800-5 (red), and 800-10 (black).

was found between '800-5' and '800-10'.

2-2. XRD Analysis

The surface chemical characteristics of prepared activated carbons were revealed by XRD. From the result shown in Fig. 4, Cu (PDF number 04-0836, Cu) and some CuOx (PDF number 05-0667, Cu2+1O) were found to be bound on modified sorbent surface. These could be considered as Cu with a bit of doped O. It was related to the activation reaction ($C+CO_2 \rightarrow 2CO$); the existence of reducing CO might be the reason why Cu was bound on the surface. When the preparation process was over and the activated carbon was exposed to air, part of active Cu on surface could be reacted with O_2. So Cu with a bit of doped O was found impregnated on the surface of activated carbon. No significant intensity difference was observed between the samples prepared from two different $CuCl_2$ concentrations. Besides, inactive substances SiO_2 (PDF number 46-1045, SiO_2), $CaSi_2O_5$ (PDF number 51-0092, $CaSi_2O_5$), CaO (PDF number 37-1497, CaO) and $CaCO_3$ (PDF number 47-1743, $CaCO_3$) were found in the carbon material and activated carbons.

3. Capability of Gaseous Hg^0 Adsorption

The Hg removal rates of prepared activated carbons were tested and compared with that of commercial activated carbons: Norit LH and FGD.

The total Hg removal efficiency η_{Hg}, and adsorption rate η_{ads} within an experiment were defined as follows:

$$\eta_{Hg} = (c_{in}^{Hg^0} \times t - \int c_{out}^{Hg^0} dt) / c_{in}^{Hg^0} \times t \quad (2)$$

$$\eta_{ads} = m^{Hg^P} / (c_{in}^{Hg^0} \times t \times v) \quad (3)$$

where $c_{in}^{Hg^0}$, $c_{out}^{Hg^0}$ represent the gaseous Hg concentration in flue gas at reactor inlet and outlet, m^{Hg^P}, t and v represent the mass of Hg adsorbed, the adsorption time and carrier gas flow rate, respectively.

The Hg balance was established to verify the reliability of Hg collection and measurement during experiments. The balance rate of Hg within a certain time is defined as follows:

$$\eta_{blance}^{Hg} = (m^{Hg^P} + \int c_{out}^{Hg^0} \times v dt) / (c_{in}^{Hg^0} \times t \times v) \quad (4)$$

Table 3 presents the Hg balance obtained from experiments. The balances ranged from 74.4% to 97.3%. Considering the difficulties in low Hg concentration measurement, the experimental error is acceptable [14].

The reaction time of 1 hour was chosen. Fig. 5 shows the Hg removal by prepared and commercial activated carbons in 1 hour. As can be seen, the Hg removal of functionalized activated carbon was much higher than that of the non-functionalized activated carbon. The '700-10' and '800-5' samples adsorbed about 80% of total gaseous Hg, which is very close to the Hg removal rate of Norit

Table 3. Balance of Hg adsorption by different activated carbon samples

Activated carbon	600	700	800	900	600-5	700-5	800-5	900-5	600-10	700-10	800-10	900-10
Balance, %	84.0±9.6	91.3±6.0	85.2±6.8	83.9±5.2	88.5±0.3	82.6±2.6	84.8±8.1	89.8±0.2	81.5±6.5	83.6±0.7	90.4±2.2	82.6±3.7

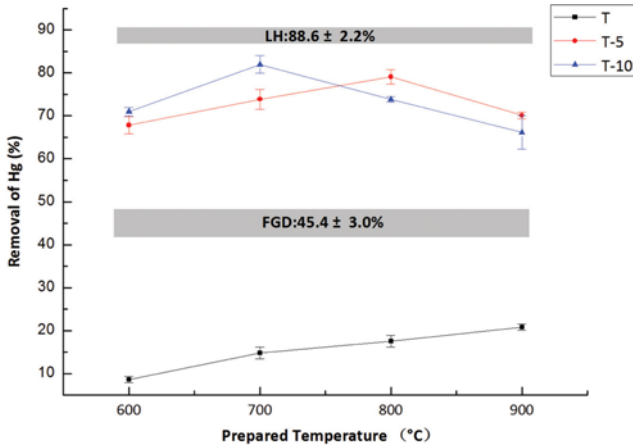

Fig. 5. Hg Removal by different activated carbon samples within 1 h (X was the prepared temperature).

LH (88.6±2.2%) and higher than Norit FGD (45.4±3.0%). No significant difference was observed between the samples prepared from different $CuCl_2$ concentrations.

Gaseous Hg was adsorbed by both physical and chemical adsorption. The physical adsorption was due to the van der Waals force from activated carbon's micropore, whilst the chemistry adsorption was caused by strong interaction such as chemical bond [15].

For non-functionalized activated carbon '600', '700', '800' and '900', the Hg removal rate (8.57%-20.8%) increased with surface area and pore volume, but was much lower than that of functionalized activated carbons prepared from the same process (67.8%-82.0%). The adsorption of non-functionalized activated carbon could be explained by physical adsorption.

But for '600-5', '700-5', '800-5' and '900-5' (or similarly '600-10', '700-10', '800-10' and '900-10'), the removal rate was apparently not relevant to physical properties such as surface area and pore volume. The adsorption of Hg for functionalized activated carbon could be explained as a chemical adsorption process, as discussed in the next section. The Hg removal rate for '600-5' and '600-10' whose physical structures were less developed (as shown in Table 1) was as high as 67.8% and 71.0%, respectively. This demonstrates the potential of the prepared sorbents in industrial applications, taking into account that these types of sorbents were prepared under even lower temperature and with simplified one-step preparation process. As characterized previously, the active species on the functionalized active carbon should be Cu with a little bit doped O.

DENSITY FUNCTIONAL THEORY ANALYSIS

Due to the very low mass fraction of Hg in sorbent (usually much less than 1% wt), it was extremely difficult to identify the reaction pathways between Hg and active chemical species by traditional surface characterization means. Many researches [16-18] had confirmed that the quantum chemistry calculation using the method of density functional theory (DFT) could be a promising way to understand the adsorption of gaseous Hg on sorbent surface. In this study, DFT calculation was also adopted to explore the adsorption mechanisms and fundamental chemical reactivity of Hg on the surface of the developed sorbent.

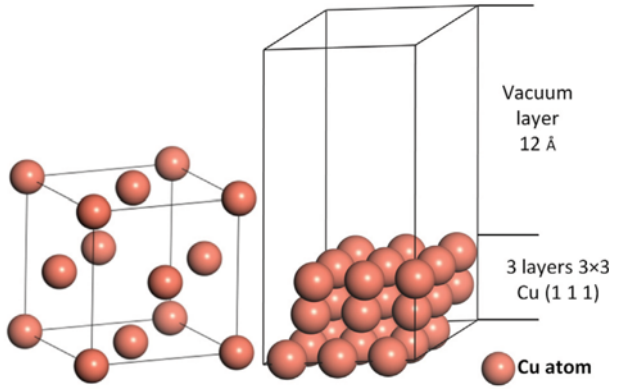

Fig. 6. Cu bulk and Cu clusters model.

1. Method

All the DFT calculations in this study used first-principles calculations with the Cambridge Sequential Total Energy Package [19,20] of Material Studio. The generalized gradient approximation (GGA) scheme and Perdew-Burke-Ernzerhof (PBE) [21] functional was used to describe the energy of exchange and correlation interactions. The interaction between electron and ionic core was described by ultra-soft pseudo potentials.

The electronic wave functions were expanded on a plane wave basis with a cut-off energy of 400 eV. The convergence criteria included a) self-consistent field (SCF) of 1.0×10^{-6} eV/atom, b) energy of 1×10^{-5} eV/atom, c) displacement of 10^{-3} Å, d) force of 0.03 eV/Å, and e) stress of 0.05 GPa.

For bulk lattice (Fig. 6), energies were converged with (8×8×8) k point in a Monhorst-pack grid [22]. The lattice parameter for bulk Cu was calculated to be 3.629 Å, which was in good agreement with the value of 3.636 Å [23] and 3.637 Å [24] from other researches, suggesting the computational setup was appropriate.

Researches already showed that Cu(111) was a promising surface that could be used to represent Cu surface properties [25]. Considering the computational speed and surface properties, a three-layered (3×3) unit cell of Cu(111) slab was modeled (Fig. 6). The vacuum region between slabs was set to 12 Å to avoid the interactions between periodic images [26]. The surface Brillouin zone integration was calculated using 4×4×2 k point Monhorst-pack meshes. The surface layer of atoms were relaxed, while the rest layers were fixed.

The equilibrium geometries of Hg and O_2 were all examined in a large cell of 10×10×10 $Å^3$ periodic box. The calculated bond distances of O_2 was 1.24 Å, which agreed well with the previous research of 1.114-1.247 Å [27].

The adsorption energy (E_{ads}) was defined as follows:

$$E_{ads}=E_{adsorbate-substrate}-(E_{adsorbate}+E_{substrate}) \quad (5)$$

where $E_{adsorbate-substrate}$ is the total energy of the adsorbate/substrate system, $E_{adsorbate}$ is the total energy of the isolated adsorbate at its equilibrium geometry, and $E_{substrate}$ is the total energy of substrate. A negative E_{ads} value corresponds to a stable adsorbate/substrate system.

2. Hg Adsorption on Cu(111) Surface

A single Hg atom was placed on three different adsorption sites

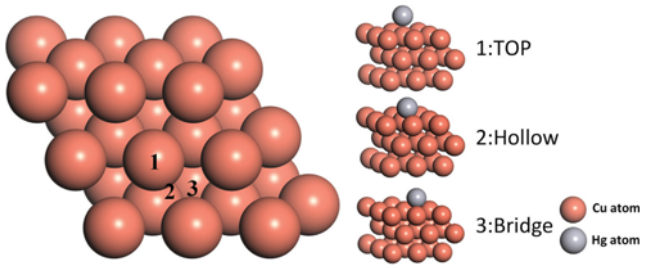

Fig. 7. Schematic top view of adsorption sites for the Cu(111) surface and 3 stable adsorption sites.

Table 4. Adsorption energy E_{ads} (kJ/mol) and distance $R_{Hg\text{-}Cu}$ (Å)

Adsorption sites	E_{ads} kJ/mol	$R_{Hg\text{-}Cu}$ Å
1	−37.5	2.664
2	−44.6	1.964
3	−46.6	2.810

(Fig. 7), referred to as a coverage of 1/9 ML. The calculated adsorption energy and distance are given in Table 4. The results show that the stability of Hg adsorption was in the order of top(1)<bridge(2)<hollow(3). The hollow site was found to be the most energetically preferred adsorption position with the lowest adsorption energy of –46.6 kJ/mol. The adsorption could be concluded as chemical adsorption.

Partial density of states (PDOS) was also applied to analyze the adsorption mechanism. The partial density of states showed the number of occupied electrons per interval of energy at each energy level [28].

The PDOS of Hg is presented in Fig. 8. The isolated Hg atoms are represented by s, p and d state, where s state has two peaks at −0.001 eV and 6.938 eV, p state has one peak at −5.766 eV and d state has one peak at –3.058 eV. The result is in consistent with previous research [29], except that only one peak was observed at d state in our research, whereas an extra peak was found by Zhang et al.

After adsorption, the PDOS of Hg atom at s, p and d state was changed at adsorption site 1 (top), 2 (bridge), and 3 (hollow). The *s* state electrons energy peaks at adsorption site 1, 2 and 3 shifted to the lower energy of –3.722 eV, –4.052 eV and –4.114 eV, respectively; at p state, the energy peaks of adsorption sites 1, 2 and 3 decreased to about −1.800 eV; at d state, the electrons energy peak at adsorption Site 1, 2 and 3 decreased to –6.040 eV, –6.336 eV, –6.404 eV. The decrease of energy peak proved the adsorbed Hg was stable, so that the Hg was more stable at hollow site than bridge site than top site, which is in consistent with the adsorption energy and distance above. According to the PDOS absolute value and the variation, it could be found that the *d* state (original energy of −4 eV to −2 eV) of Hg mainly participated in the reaction on Cu(111) surface.

3. Hg adsorbed on Cu(111) with Doped O

According to surface chemical characteristic analysis (XRD analysis), a model of single O atom doped on the surface of Cu(111) was proposed (Fig. 9). Similar to one Hg atom absorbed on Cu(111) surface, the most stable structure of single O doped on the surface of Cu(111) was at the hollow structure. The computation setup was the same as that of Hg adsorption on Cu(111).

As shown in Fig. 9, eight possible adsorption sites were investigated. The calculation found that the stable adsorption sites were sites 1 and 8. The calculated adsorption energy and distance are given in Table 5. Site 8 was found to be the most energy preferred adsorption position with an adsorption energy of –50.4 kJ/mol. The adsorption could be considered as chemical adsorption.

Compared with the adsorption energy (−46.6 kJ/mol) and adsorption distance (2.810 Å) on Cu(111), it could be inferred that

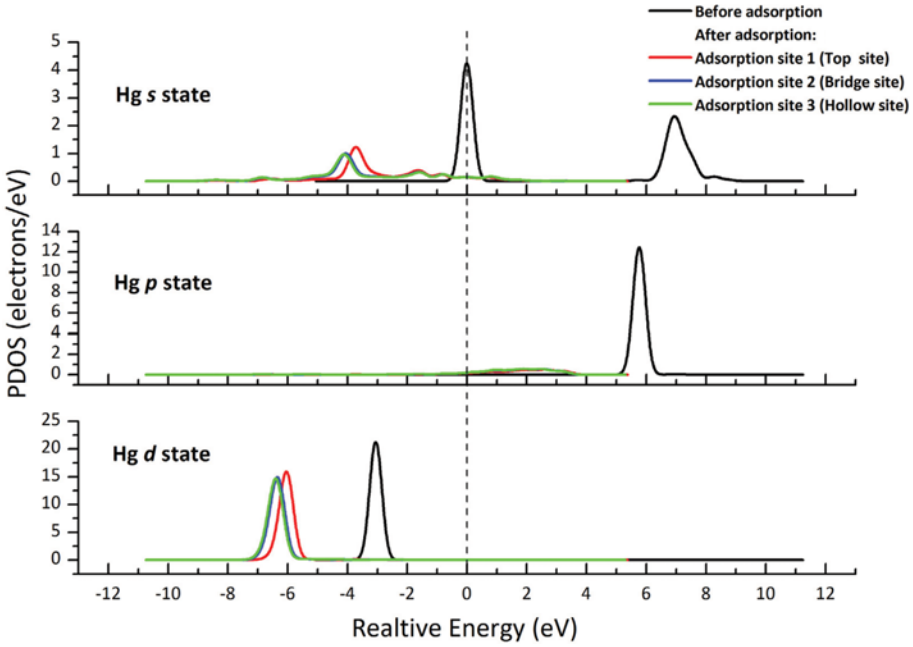

Fig. 8. PDOS of Hg absorbed on the surface of Cu(111), the fermi level is set to be zero (dashed line).

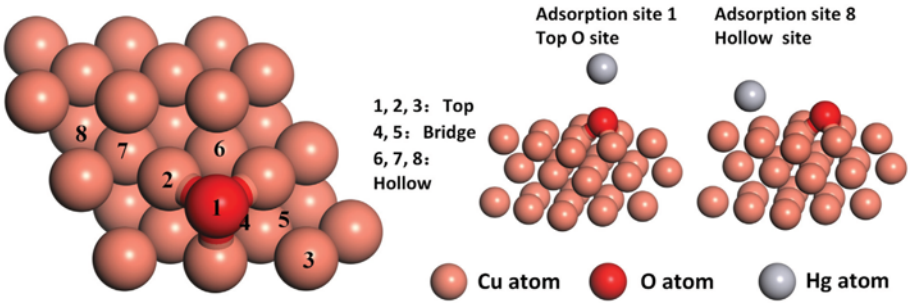

Fig. 9. Schematic top view of adsorption sites for the doped O on Cu(111) surface and the stable adsorption Site 1(left) and 7 (right).

Table 5. Adsorption energy E_{ads} (kJ/mol) and distance R (Å)

Adsorption sites	E_{ads} kJ/mol	R Å
1 (O top site)	−10.1	3.244 Hg-O
8 (Hollow site)	−50.4	2.795 Hg-Cu

the doped O accelerated the adsorption of Hg on neighboring hollow site.

As shown in Fig. 10, PDOS of Hg atom changed after adsorption. It was obvious that the electron's energy (s, p, d state) at site 8 was lower than that at site 1. It proved that the hollow site (close to O atom) was the most stable adsorption site. According to the PDOS absolute value and the variation, it could be found that the d state electrons (original energy of −4 eV to −2 eV) of Hg participated in the reaction on the surface of Cu(111) with doped O. The peak of d state energy of Hg on Cu(111) with doped O was a bit lower than that of the Hg atom on Cu(111). From the available analytical results, it is difficult to explain why the doped O accelerates the adsorption of Hg. The influence of doped O on surface properties needs to be investigated.

As shown in Fig. 10, the surface PDOS was mainly concentrated on d state, which is a typical density of state property of transition metal. The original energy of d state of Cu(111) and Cu(111) with doped O was about −1 eV to −5 eV, which agreed with the energy of d state (−4 eV to −2 eV) of Hg. The d state electrons on Cu(111) surface decreased after adsorption. This phenomenon could be explained by the energy approximation principle of molecular orbital theory. The result revealed that the adsorption of Hg on Cu(111) or Cu(111) with doped O was mainly caused by the orbital hybridization between the d state electrons of sorbent surface and Hg. There was no PDOS evidence to support the assumption that the doped O accelerated the Hg adsorption. Hence, the change of physical properties on sorbent surface might be a possible reason. Through chemical calculation, it was found that the average Cu-Cu bond length (excluding the 3 Cu atoms connected with O) on surface decreased from 2.5200 Å to 2.5166 Å after O doped. The shorter Cu-Cu distance actually caused the Hg atom at hollow site

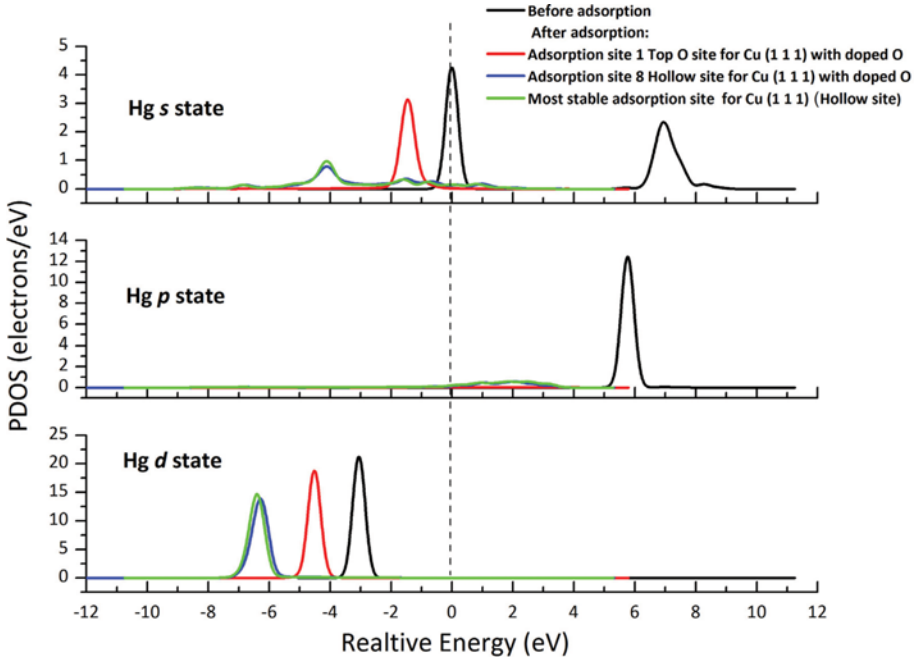

Fig. 10. PDOS of Hg absorbed on the surface of Cu(111) with one doped O. The fermi level is set to be zero (dashed line).

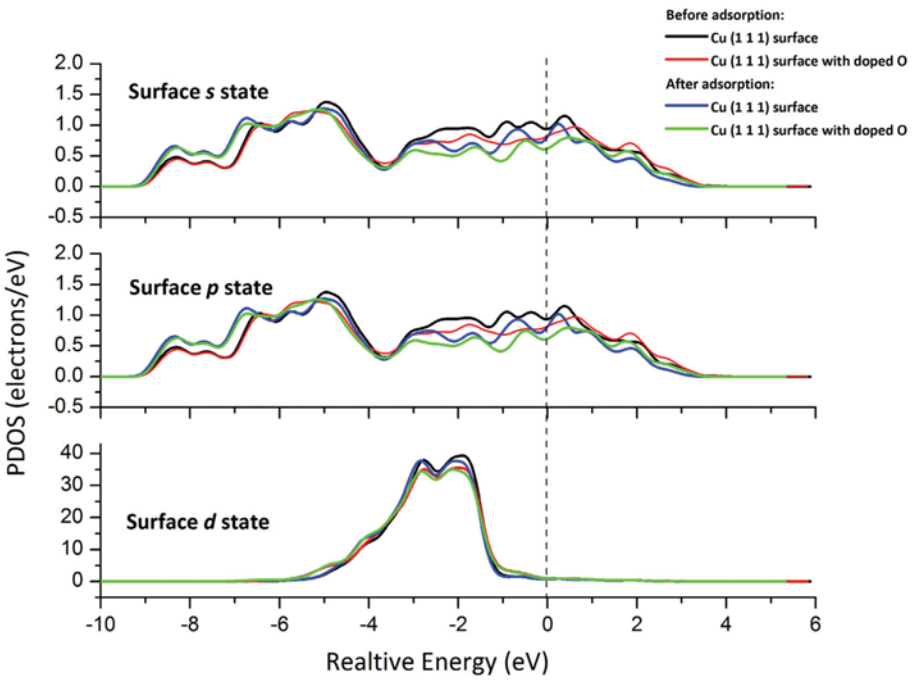

Fig. 11. PDOS of Cu(111) surface (9 Cu atoms) and Cu(111) surface with one doped O (9 Cu atoms and one O atom).

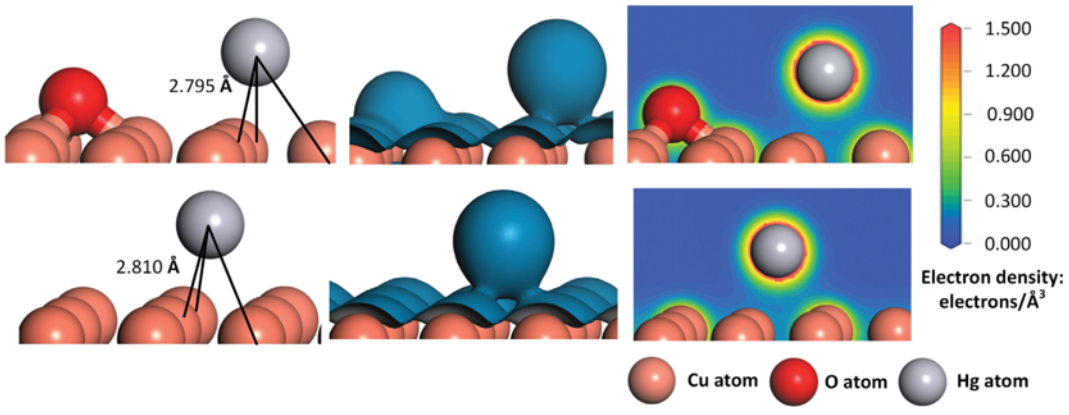

Fig. 12. Electrons density for the adsorption of Hg on Cu(111) surface and Cu(111) surface with one doped O.

closer to the 3 Cu atoms, which could be the reason for adsorption acceleration by doped O.

The electron density cloud was also plotted to reveal the adsorption (Fig. 11). It was straightforward to identify the overlap among electrons of Hg and 3 Cu atoms on either original or O-doped Cu(111) surface.

CONCLUSION

The preparation of Cu-impregnated activated carbons can be simplified by combining activation and functionalization into one-step preparation. $CuCl_2$ can enhance the carbon activation, improving surface area up to 30.6-32.8%, and pore volume up to 29.0%-43.0%. Cu with doped O was supported on carbon surface under 600 °C. The sorbent developed achieved high Hg removal rate (67.8%-82.0%), which was very close to that of commercial activated carbon of Norit FGD (45.4±3.0%) and LH (88.6±2.2%). This type of activated carbon preparation is potentially useful for future industrial applications.

Quantum chemistry calculation revealed that the adsorption of Hg on Cu(111) with or without doped O was chemical adsorption. The adsorption was mainly caused by the orbital hybridization between the d state electrons of surface Cu and the d state electrons of Hg. The adsorption energy at Cu(111) was −47.7 kJ/mol while at Cu(111) with doped O was −50.4 kJ/mol. The doped O improved the adsorption of Hg due to the change of surface physical properties, i.e., reducing the Cu-Cu distance.

ACKNOWLEDGEMENTS

This work was financially supported by China National Natural Science Foundation via project No. 51376109.

REFERENCES

1. .M. C. Houston, *J. Clin. Hypertens.*, **13**, 621 (2011).
2. United Nations Environment Programme, *The Global Hg Assessment 2013*, Switzerland (2013).
3. Q. Zhou, Y. Duan, C. Zhu, J. Zhang, M. She, H. Wei and Y. Hong, *Korean J. Chem. Eng.*, **32**, 1405 (2015).
4. Natural Resources Defense Council, *Summary of Recent Mercury Emission Limits for Power Plants in the United States and China*, Unites States and China (2012).
5. A. P. Jones, J. W. Hoffmann, D. N. Smith, T. J. Feeley and J. T. Murphy, *Environ. Sci. Technol.*, **41**, 1365 (2007).
6. H. Yang, Z. Xu, M. Fan, A. E. Bland and R. R. Judkins, *J. Hazard. Mater.*, **146**, 1 (2007).
7. H. Hadoun, Z. Sadaoui, N. Souami, D. Sahel and I. Toumert, *Appl. Surf. Sci.*, **280**, 1 (2013).
8. S. A. Dastgheib, J. Ren, M. Rostam-Abadi and R. Chang, *Appl. Surf. Sci.*, **290**, 92 (2014).
9. C. Chiu et al., *Aerosol Air Qual. Res.*, **2094**, 15 (2015).
10. L. Zhang, Y. Zhuo, W. Du, Y. Tao, C. Chen and X. Xu, *Ind. Eng. Chem. Res.*, **51**, 5292 (2012).
11. J. F. González, S. Román, C. M. González-García, J. M. V. Nabais and A. L. Ortiz, *Ind. Eng. Chem. Res.*, **48**, 7474 (2009).
12. J. D. Laumb, S. A. Benson and E. A. Olson, *Fuel Process. Technol.*, **85**, 577 (2004).
13. R. Landreth, S. Nelson, X. Liu, Z. Tang, A. Overholt and L. Brickett, *World of Coal Ash* (2007).
14. F. Goodarzi, *J. Environ. Monit.*, **6**, 792 (2004).
15. J. Wang, F. Xue, Y. Liu, *Physical chemistry*, Tsinghua University Press, Beijing (1992).
16. L. Tao, X. Guo and C. Zheng, *P. Combust. Inst.*, **34**, 2803 (2013).
17. J. A. Steckel, *Phys. Rev. B.*, **77**, 115412 (2008).
18. L. Geng, L. Han, W. Cen, J. Wang, L. Chang, D. Kong and G. Feng, *Appl. Surf. Sci.*, **321**, 30 (2014).
19. M. D. Segall, P. Lindan, M. J. Probert, C. J. Pickard, P. J. Hasnip, S. J. Clark and M. C. Payne, *J. Phys.-Condens. Mat.*, **14**, 2717 (2002).
20. S. J. Clark, M. D. Segall, C. J. Pickard, P. J. Hasnip, M. J. Probert, K. Refson and M. C. Payne, *Z. Kristallogr.*, **220**, 567 (2005).
21. J. P. Perdew, K. Burke and M. Ernzerhof, *Phys. Rev. Lett.*, **77**, 3865 (1996).
22. H. J. Monkhorst and J. D. Pack, *Phys. Rev. B.*, **13**, 5188 (1976).
23. S. Ramos De Debiaggi, G. F. Cabeza, C. D. Toro, A. M. Monti, S. Sommadossi and A. F. Guillermet, *J. Alloy. Compd.*, **509**, 3238 (2011).
24. K. Lejaeghere, V. Van Speybroeck, G. Van Oost and S. Cottenier, *Crit. Rev. Solid State*, **39**, 1 (2014).
25. A. Soon, M. Todorova, B. Delley and C. Stampfl, *Phys. Rev. B.*, **73** (2006).
26. B. Zhang, J. Liu, C. Zheng and M. Chang, *Chem. Eng. J.*, **256**, 93 (2014).
27. A. E. Reed, F. Weinhold, L. A. Curtiss and D. J. Pochatko, *J. Chem. Phys.*, **84**, 5687 (1986).
28. W. Xiang, J. Liu, M. Chang and C. Zheng, *Chem. Eng. J.*, **200-202**, 91 (2012).
29. B. Zhang, J. Liu, C. Zheng and M. Chang, *Chem. Eng. J.*, **256**, 93 (2014).